J Mater Sci (2008) 43:5924–5929
DOI 10.1007/s10853-008-2872-y

Synthesis and characterization of anatase and rutile TiO_2 nanorods by template-assisted method

A. Sadeghzadeh Attar · M. Sasani Ghamsari · F. Hajiesmaeilbaigi · Sh. Mirdamadi · K. Katagiri · K. Koumoto

Received: 14 April 2008 / Accepted: 10 July 2008 / Published online: 27 July 2008

Abstract Well-aligned anatase and rutile TiO_2 nanorods and nanotubes with a diameter of about 80–130 nm have successfully been fabricated via sol-gel template method. The prepared samples were characterized by using thermogravimetric (TG) and differential thermal analysis (DTA), X-ray diffraction (XRD), scanning electron microscopy (SEM), transmission electron microscopy (TEM), and energy dispersive X-ray spectroscopy (EDS). The XRD results indicated that the TiO_2 nanorods were crystallized in the anatase and rutile phases, after annealing at 400–800 °C for different periods of time from 0.2 to 10 h.

Introduction

Titanium dioxide is a fascinating class of inorganic solids used in a wide range of common and high technique applications because of its moderate price, chemical stability, non-toxicity, biocompatible, very high reflectivity of light, efficient photocatalysis, and surface reactivity [1–4]. These properties can be controlled by TiO_2 crystal structure, crystallite size, size distribution, and morphology [5–7]. Crystalline TiO_2 exists in three polymorphic forms: anatase (tetragonal, $c/a > 1$), rutile (tetragonal, $c/a < 1$), and brookite (orthorhombic) [7–11]. Rutile is the thermodynamically stable phase (generally in the 600–1855 °C), whereas anatase and brookite are metastable and are readily transformed to rutile when heated. The phase change from anatase to rutile has been reported to occur in different temperature ranges from 600 °C to 1100 °C, depending on the preparation conditions, particle size, and the presence of impurities [11–13]. Anatase TiO_2 has been widely studied due to its tremendous technological importance in various applications. Anatase TiO_2 has the (101) plane as the most exposed face in nanocrystals [8, 14]. About rutile TiO_2, the (110) face has been shown to be the exposed plane. In this case, the TiO_2 (110) plane yields defect stoichiometry leading to a Ti^{3+} site, which is photocatalytically active [8, 15]. The basic difference between anatase and rutile is the symmetry about oxygen atoms as well as differences in the polarization of the oxygen ions [8].

TiO_2 nanostructures are experiencing a rapid development in recent years due to their unique properties that are derived from their surface areas compared to TiO_2 bulk material. One of the ways of enhancing the surface area of nanostructured TiO_2 material is to convert it into one-dimensional (1D) nanostructures such as nanorods, nanowires, and nanotubes. These structures have larger surface areas than their particulate forms and have gained considerable attention for their brilliant prospects in photocatalysts, gas and humidity sensors, environment purification, photovoltaic cells, and photoelectrochromic windows [5, 6, 16–22]. Numerous methods have been developed for the synthesis of 1-D nanostructures including chemical vapor deposition (CVD) [23], electron beam lithography [24], surfactant-directed [25], and the filling of templates with colloidal oxide particles

A. Sadeghzadeh Attar · Sh. Mirdamadi (✉)
Department of Metallurgy and Materials Engineering, Iran University of Science and Technology, Tehran, Iran
e-mail: mirdamadi@iust.ac.ir; ab_sadeghzadeh@yahoo.com

M. Sasani Ghamsari · F. Hajiesmaeilbaigi
Solid State Lasers Research Group, Laser and Optics Research School, Tehran 11365-8486, Iran

K. Katagiri · K. Koumoto
Department of Applied Chemistry, Graduate School of Engineering, Nagoya University, Nagoya 464-8603, Japan

[26–28]. Among them, the template-assisted synthesis method has been found as an effective way for the formation of 1-D nanostructures [29, 30]. This approach combines the sol-gel processing and template-based growth. In this manner, the template is dipped directly into the prepared TiO_2-sol solution by sol-gel process for a required period.

This paper reports the growth and characterization of anatase and rutile TiO_2 nanorods/nanotubes by a template-assisted sol-gel method. Also, the effects of annealing temperature and time on the phase structure of TiO_2 nanorods are reported.

Experimental

The precursor chemicals for preparation of TiO_2-sol were used as-received: titanium tetraisopropoxide (≥99%, Kishida), acetylacetone (≥99%, Kishida), ethyl alcohol (99.5%, Kishida), and deionized water. Titanium tetraisopropoxide was added to a reaction beaker in the presence of ethanol. Acetylacetone was added into ethanol and water in a separate beaker. Then, two resulting solutions were mixed and stirred at room temperature for 2 h.

For the synthesis of TiO_2 nanorods/nanotubes, the porous anodic alumina membranes (Anodisc; Whatman Inc.) were used as the template. The diameter, average thickness, and pore size of these templates were 21 mm, 60 μm, and 100–150 nm, respectively. At first, the prepared TiO_2-sol was injected by a syringe into the templates several times. Then, the templates were withdrawn from the solution and were dried in air for 24 h. The prepared samples were kept at 100 °C for 8 h to remove the residual water and alcohol. For the preparation of anatase and rutile TiO_2, the samples were gradually heated up at a rate of 2 °C/min in 300, 400, 500, 600, 700, and 800 °C and were held at this temperature for various periods of time: 0.2, 0.5, 1, 2, 4, and 10 h. Finally, the furnace was shut down and the samples were cooled down to room temperature. Figure 1 shows the details of heat-treatment schedule for rutile and anatase TiO_2.

Thermogravimetric and differential thermal analysis (Thermo Plus TG8120, Rigaku) were carried out in air from room temperature up to 1000 °C, with a heating rate of 2 °C/min in a Pt crucible. The crystalline phase of TiO_2 samples were characterized by XRD with the use of a Rigaku X-ray diffractometer Rint 2100. For XRD, Cu Kα radiation was used at 40 kV and 30 mA, with a step size of 0.02 from 20 to 80. The surface morphology and cross-section of the alumina template was obtained by using a field emission-scanning electron microscopic (FE-SEM; Model JSM-6330F, JEOL). The microstructure of obtained TiO_2 nanorods and nanotubes was observed by scanning electron microscopy (SEM; Model S-3000N, Hitachi, Japan) and transmission electron microscopy (TEM; Model H-800, Hitachi, 200 kV). The SEM and TEM samples were prepared by dissolving alumina template in 1 and 6 M NaOH aqueous solutions, respectively. Then the samples were washed several times with distilled water to remove the dissolved alumina and the remaining NaOH solution.

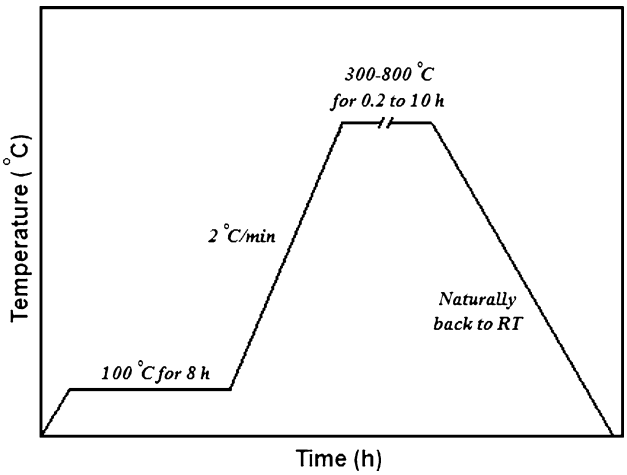

Fig. 1 The heat-treatment program for the preparation of anatase and rutile TiO_2 nanorods/nanotubes

Results and discussion

The TG-DTA curves of the as-prepared TiO_2 materials are shown in Fig. 2. The endothermic peak at about 40–120 °C represents the removal of adsorbed water and solvent. On DTA curve in Fig. 2, the exothermic peaks appear at 200–400 °C that are attributed to the combustion of organic compound, acetylacetanate groups, and the formation of anatase phase. The final small loss step above 550 °C is

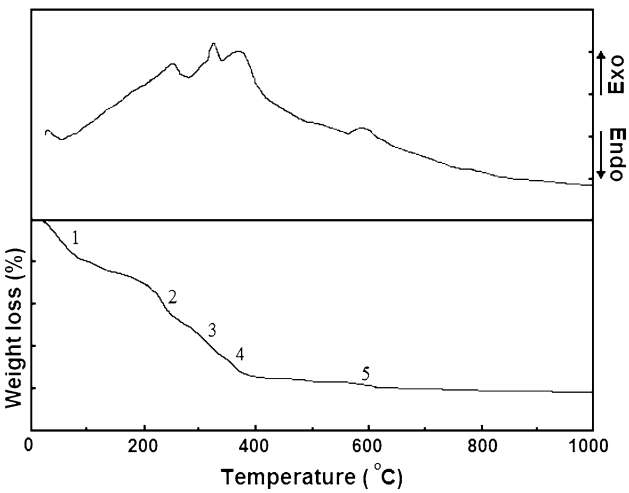

Fig. 2 TG-DTA curves of the as-prepared TiO_2 nanorods

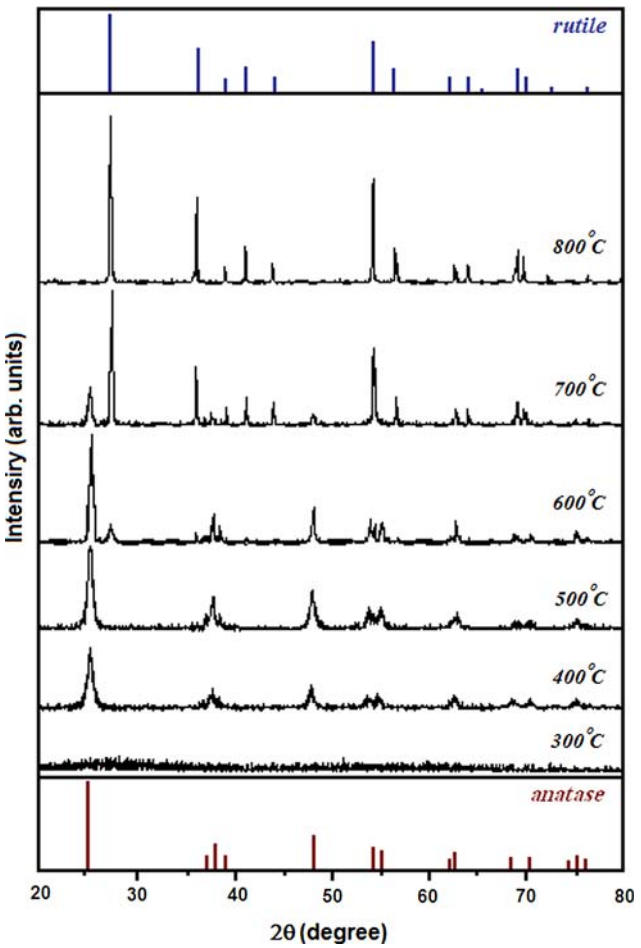

Fig. 3 XRD patterns of the TiO_2 nanorod arrays annealed at various temperatures for 2 h

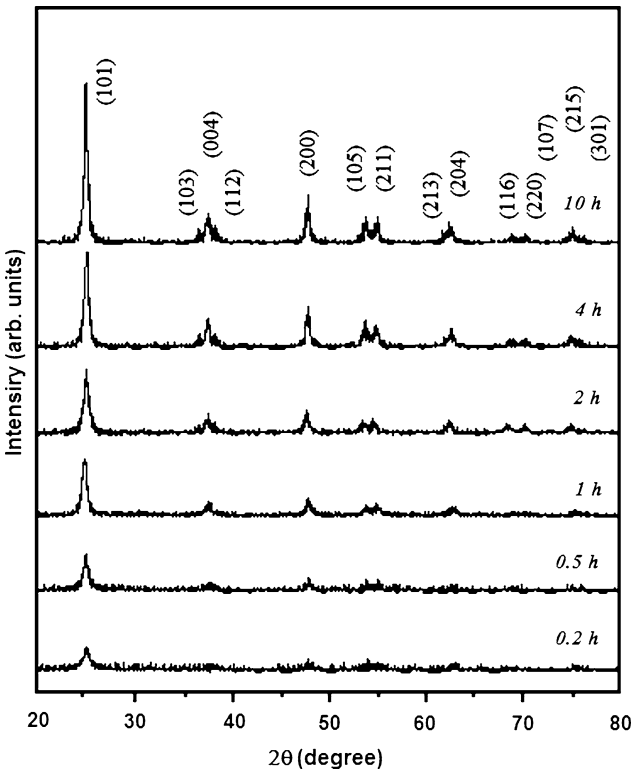

Fig. 4 XRD patterns of the TiO_2 nanorod arrays annealed at 400 °C for different times

also an exothermic reaction, obviously corresponding to the crystallization of the rutile phase.

The XRD patterns for TiO_2 nanorod arrays annealed at various temperatures and times are shown in Figs. 3 and 4. In Fig. 3, we indicate XRD spectra of TiO_2 nanorods annealed at different temperatures for 2 h in air atmosphere. The TiO_2 samples annealed at 300 °C showed no peaks, while the XRD patterns of the samples annealed at 400 and 500 °C are characteristic of anatase TiO_2. In the range from 400 °C to 500 °C, only anatase phase is obtained. The formation of anatase TiO_2 is found to begin below 400 °C, indicating the start of the amorphous to anatase crystallization, which coincides well with TG-DTA results in Fig. 2. When the annealing temperature is around 600 °C, rutile phase peaks appear. It can be found the transformation temperature of anatase to rutile is approximately 600 °C, while some small diffraction peaks of anatase were also observed. With increasing temperature to 700 °C, the amount of rutile phase increases and at 800 °C, rutile is a main phase and anatase disappears. This shows that transformation of anatase to rutile phase is complete below this temperature. For the prepared TiO_2 samples, with increasing annealing temperature from 400 °C to 800 °C, the peak intensities of anatase and rutile increase. The diffraction peaks of anatase and rutile become narrower and their crystallity is enhanced. The crystallite sizes of the TiO_2 nanorods annealed at various temperatures were evaluated and are summarized in Table 1. The crystallite size measurements were carried out using the Debye-Scherrer's equation [31]:

$$D = \frac{0.89\lambda}{\beta \cos\theta}$$

Table 1 Average crystallite size obtained from XRD results for TiO_2 nanorods annealed at various temperatures for 2 h

Annealing temperature (°C)	Average crystallite size[a] (nm)	
	Anatase	Rutile
300	–	–
400	11	–
500	13	–
600	17	23
700	22	27
800	–	35

[a] Calculated by (101) for anatase and (110) for rutile

where D is crystallite size, λ is wavelength of the X-ray, β is the full-width at half-maximum (FWHM) intensity (obtained after correction for the instrumental broadening), and θ is the angle of diffraction. The (101) diffraction peak is used for anatase phase and (110) peak for rutile phase. It can be seen in Table 1 that the average crystallite size of the anatase and rutile samples increased from 11 to 35 nm as the annealing temperature increased from 400 °C to 800 °C. At higher annealing temperature, the crystallites formed are larger in size, which can be attributed to the thermally promoted crystallite growth. It is well known that the annealing improves the crystallity, and the amorphous TiO_2 to the anatase phase and after that anatase changes to the rutile phase with increasing temperature [32].

Figure 4 shows XRD pattern of TiO_2 nanorods annealed at 400 °C for various periods of time. A pronounced (101) peak of TiO_2 at $2\theta = 25.3^\circ$ was observed that corresponds to the tetragonal anatase single phase. Similar crystal structure was observed for the samples annealed at 400 °C for all cases. With increasing annealing time, the peak intensity of the (101) diffraction increases and its width becomes narrower. Figure 5 demonstrates the average crystallite size of anatase phase as a function of annealing time. The size of anatase crystallites increases from 9 to 15 nm, when the annealing time is raised from 0.2 to 10 h.

Figure 6a and b shows FE-SEM images of the surface structure and cross-sectional structure of anodic alumina membrane as the starting material. It can be seen that this template has many pores whose mean diameter is approximately 100–150 nm. SEM photographs of the anatase TiO_2 nanotube and nanorod arrays obtained by annealing at 400 °C for 2 h are shown in Fig. 7a and b, respectively. Figure 7a indicates image of the TiO_2 nanotubes that are arranged roughly parallel to one another and

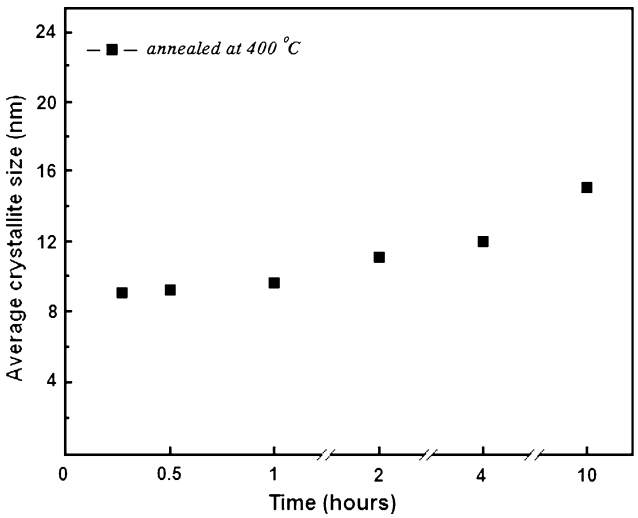

Fig. 5 Average crystallite size of anatase phase as function of annealing time

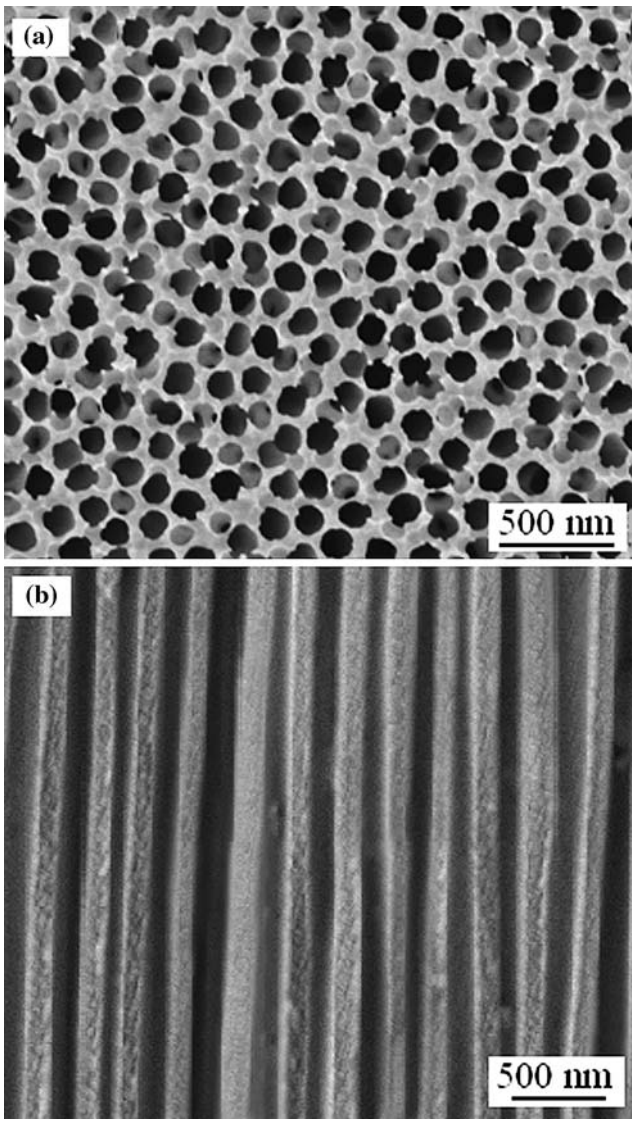

Fig. 6 FE-SEM images of the (**a**) surface structure and (**b**) cross-sectional structure of the anodic alumina membrane

highly uniform in diameter. Densely assembled nanorods with a diameter of about 80–130 nm and length of several micrometers were observed in Fig. 7b, which corresponds to approximately 15–20% lateral shrinkage with respect to the template pore diameter. This size difference is almost due to the volume shrinkage caused by removal of residual materials and densification during the annealing. The prepared TiO_2 nanorod and nanotube arrays are abundant, uniform, and highly ordered over a large area. In addition, we can fabricate nanorods and nanotubes with desirable diameter and length by selecting a proper template.

Figure 8a and b gives the TEM images of the TiO_2 nanotube and nanorod, respectively. The both nanotube and nanorod have a smooth morphology and longitude uniformity in diameter. It can be seen clearly in these

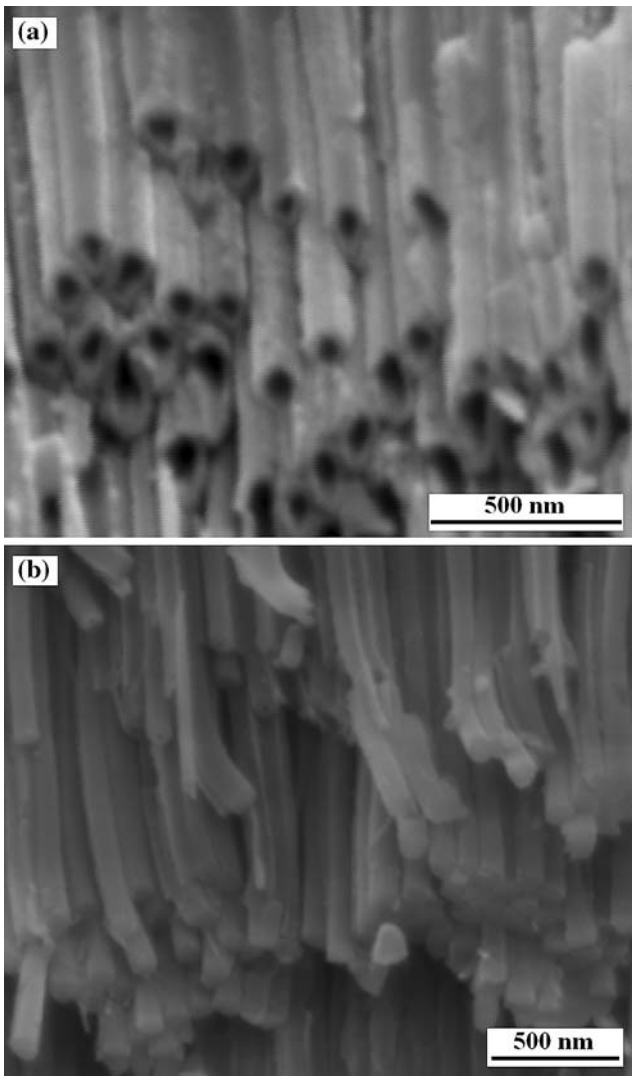

Fig. 7 SEM images of the (**a**) TiO_2 nanotubes and (**b**) TiO_2 nanorods grown into alumina templates

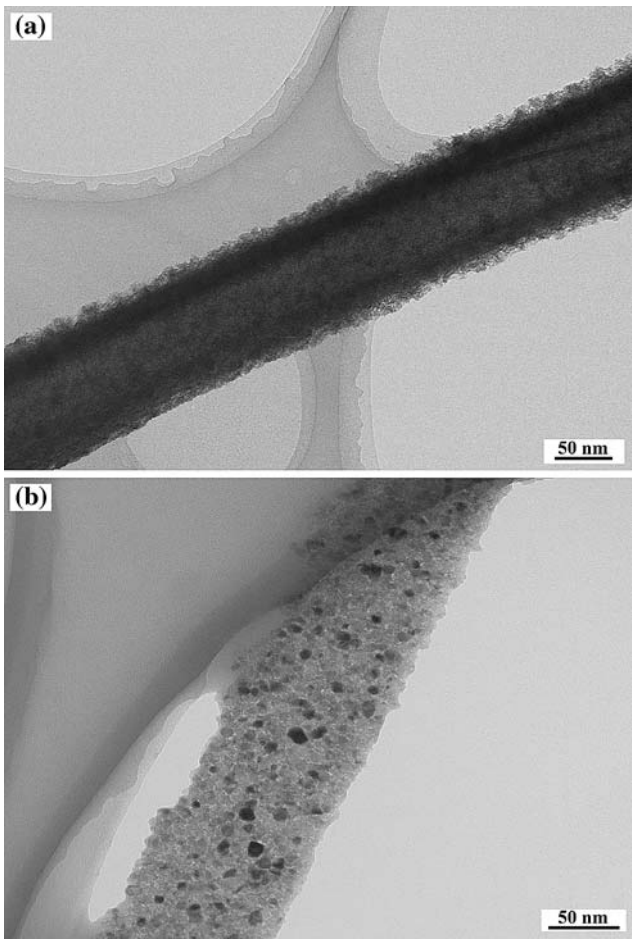

Fig. 8 TEM images of the (**a**) TiO_2 nanotube and (**b**) TiO_2 nanorod

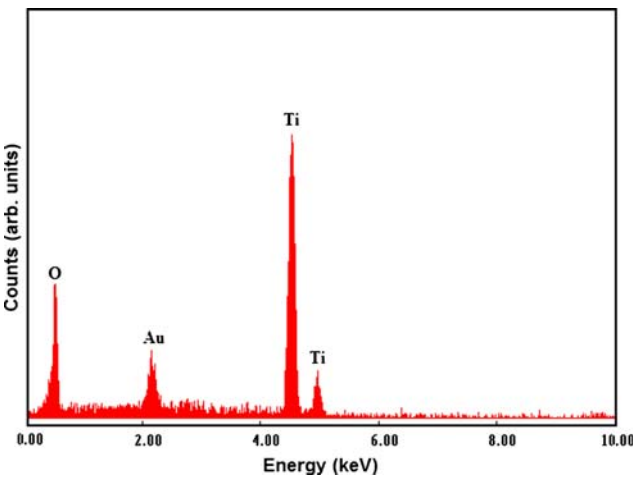

Fig. 9 EDS analysis of the TiO_2 nanorod arrays

images that the average diameter of the nanotube and nanorod is about 100 nm. The TiO_2 nanorods and nanotubes can be initiated by the formation of bonds between Ti(IV) complexes and Al-OH sites on the pore walls [33–35]. Then, the nuclei continue to grow by attracting more Ti(IV) complexes to form partly dehydrated, polymeric Ti(IV) hydroxide particles until the neighboring particles make contact with each other to produce aggregates, leading nanostructures upon annealing. The injection of the hydrolyzed TiO_2 solution by the syringe through pores of the alumina membrane has created nanochannels, which after several injections ultimately produces TiO_2 nanorods/nanotubes. After several injections, the pores became smaller, which consequently lead to the slower passage of TiO_2-sols into pores. With the immersion of the samples into boiling TiO_2-sol, the pores are completely filled, which leads to the formation of the TiO_2 nanorods and eliminates the possibility of tubes growth into template pores.

The chemical composition of the TiO_2 nanorod arrays were determined using energy dispersive X-ray spectroscopy

(EDS) that are shown in Fig. 9. EDS analysis confirms the constituent of the nanorods to be essentially Ti and O, though trace of Au is contained. The presence of peak of element Au can be ascribed to the sputter-cover on surface nanorod to provide conductibility of sample, while none of Al peak was detected in EDS analysis which firmly indicates complete removal of the alumina template.

Conclusion

In this study, the TiO_2 nanorod and nanotube arrays consisting of anatase and rutile have successfully been prepared by a sol-gel template route. It was shown that the dimension of nanorods/nanotubes depends on the pore size of the template, and their diameter is almost the same as the nominal pore size. The SEM and TEM images showed the average diameter of nanorods/nanotubes were about 100 nm in diameter with several micrometers in length. The TiO_2 nanorod arrays have the desired chemical composition with anatase and rutile crystal structures, after annealing at 400, 500, 600, 700 and 800 °C for various periods of time from 0.2 h to 10 h. From thermal analysis and XRD analysis, the anatase structure of TiO_2 appeared in annealing temperature below 400 °C and rutile structure was observed around 600 °C. The crystallite size of the obtained samples increased with increasing annealing temperature and time.

References

1. Mulmi DD, Sekiya T, Kamiya N, Kurita S, Murakami Y, Kodaira T (2004) J Phys Chem Solids 65:1181. doi:10.1016/j.jpcs.2003.12.009
2. Karvinen S, Hirva P, Pakkanen TA (2003) J Mol Struct Theochem 626:271. doi:10.1016/S0166-1280(03)00108-8
3. Xu A-W, Gao Y, Liu H-Q (2002) J Catal 207:151. doi:10.1006/jcat.2002.3539
4. Keshmiri M, Mohseni M, Troczynski T (2004) Appl Catal Environ 53:209. doi:10.1016/j.apcatb.2004.05.016
5. Niederberger M, Bartl MH, Stucky GD (2002) Chem Mater 4:4364. doi:10.1021/cm021203k
6. Wang C-C, Ying JY (1999) Chem Mater 11:3113. doi:10.1021/cm990180f
7. Wang C, Deng Z-X, Li Y (2001) Inorg Chem 40:5210. doi:10.1021/ic0101679
8. Kumar PM, Badrinarayanan S, Sastry M (2000) Thin Solid Films 358:122. doi:10.1016/S0040-6090(99)00722-1
9. Sen S, Mahanty S, Roy S, Heintz O, Bourgeois S, Chaumont D (2005) Thin Solid Films 474:245. doi:10.1016/j.tsf.2004.04.004
10. Wu J-J, Yu C-C (2004) J Phys Chem B 108:3377. doi:10.1021/jp0361935
11. Ovenstone J, Yanagisawa K (1999) Chem Mater 11:2770. doi:10.1021/cm990172z
12. Kolenko YV, Garshev AV, Churagulov BR, Boujday S, Portes P, Colbeau-Justin C (2005) J Photochem Photobiol Chem 172:19. doi:10.1016/j.jphotochem.2004.11.004
13. Djaoued Y, Bruning R, Bersani D, Lottici PP, Badilescu S (2004) Mater Lett 58:2618. doi:10.1016/j.matlet.2004.03.034
14. Banfi G, Degiorgio V, Ricard D (1998) Adv Phys 47:447. doi:10.1080/000187398243537
15. Shklover V, Nazeeruddin M-K, Zakeeruddin SM, Barbe C, Kay A, Haibach T et al (1997) Chem Mater 9:430. doi:10.1021/cm950502p
16. Francioso L, Taurino AM, Forleo A, Siciliano P (2008) Sens Actuators B 130:70. doi:10.1016/j.snb.2007.07.074
17. Hong J, Cao J, Sun J, Li H, Chen H, Wang M (2003) Chem Phys Lett 380:366. doi:10.1016/j.cplett.2003.09.037
18. Zhang Z, Wang C-C, Zakaria R, Ying JY (1998) J Phys Chem B 102:10871. doi:10.1021/jp982948±
19. Shipway AN, Katz E, Willner I (2000) ChemPhysChem 1:18. doi:10.1002/1439-7641(20000804)1:1<18::AID-CPHC18>3.0.CO;2-L
20. Wu Y, Yan H, Huang M, Messer B, Song JH, Yang P (2002) Chem Eur J 8:1260. doi:10.1002/1521-3765(20020315)8:6<1260::AID-CHEM1260>3.0.CO;2-Q
21. Boujday S, Wunsch F, Portes P, Bocquet J-F, Colbeau-Justin C (2004) Solar Energy Mater Solar Cells 83:421. doi:10.1016/j.solmat.2004.02.035
22. Jiu J, Isoda S, Wang F, Adachi M (2006) J Phys Chem B 110:2087. doi:10.1021/jp055824n
23. Pradhan SK, Reucroft PJ, Yang F, Dozier A (2003) J Cryst Growth 256:83. doi:10.1016/S0022-0248(03)01339-3
24. Zhao X-M, Xia Y, Whitesides GM (1997) J Mater Chem 7:1069. doi:10.1039/a700145b
25. Cozzoli PD, Kornowski A, Weller H (2003) J Am Chem Soc 125:14539. doi:10.1021/ja036505h
26. Lakshmi BB, Dorhout PK, Martin CR (1997) Chem Mater 9:857. doi:10.1021/cm9605577
27. Zhang M, Bando Y, Wada K (2001) J Mater Sci Lett 20:167. doi:10.1023/A:1006739713220
28. Sadeghzadeh Attar A, Mirdamadi Sh, Hajiesmaeilbaigi F, Sasani Ghamsari M (2007) J Mater Sci Technol 23:611
29. Sander M, Cote MJ, Gu W, Kile BM, Tripp CP (2004) Adv Mater 16:2052. doi:10.1002/adma.200400446
30. Mikhaylova M, Kim DK, Toprak M, Muhammed M (2003) Mat Res Soc Symp Proc 750:1
31. Cullity BD (1978) Elements of X-ray diffraction. Addison Wesley Pub, Menlo Park
32. Hong S-S, Lee MS, Park SS, Lee G-D (2003) Catal Today 87:99. doi:10.1016/j.cattod.2003.10.012
33. Diggle JW, Downie TC, Goulding C (1969) Chem Rev 69:365. doi:10.1021/cr60259a005
34. Yoon J-H, Jang S-R, Vittal R, Lee J, Kim K-J (2006) J Photochem Photobiol A: Chem 180:184. doi:10.1016/j.jphotochem.2005.10.013
35. Lakshmi BB, Patrissi CJ, Martin CR (1997) Chem Mater 9:2544. doi:10.1021/cm970268y